Chemical Engineering Journal 527 (2026) 171223

Contents lists available at ScienceDirect

Chemical Engineering Journal

journal homepage: www.elsevier.com/locate/cej

Thermal and holography imaging of heat feedback enables strategies to drive sustained combustion in highly reactive thermite composites

Lei Yang, Keren Shi, Yuxin Zhou, Mahbub Chowdhury, Afrida Anis, Michael R. Zachariah *

Department of Chemical and Environmental Engineering, University of California, Riverside, CA, 92507, USA

ARTICLE INFO

Keywords:
Mesoparticle
Carbon fiber
Digital in-line holography
Heat transfer
Combustion
Flame propagation

ABSTRACT

Nanoenergetic mesoparticles offer high energy density by integrating aluminum nanoparticles with oxidizer and a gas-generating binder; however, their superior reactivity also leads to poor heat feedback to the reaction front, resulting in poor or intermittent performance. In this work, we systematically investigated strategies to enhance heat feedback in 3D-printed sticks comprising high-loading Al–CuO–NC mesoparticles embedded in a polymer binder matrix. Specifically, we explored increasing the polymer (PMMA) binder content, adding a small fraction of carbon fibers (CFs), and varying the nitrocellulose (NC) content within the mesoparticles. Combustion behavior was characterized by high-speed digital in-line holography (DIH) to track ejected-particle size and velocity, while mechanical tests assessed the structural integrity of the composites. Increasing the binder content to 20 % eliminated the previously observed flame extinguishment/reignition oscillations and produced near-continuous combustion; however, the global burn rate remained lower than that of an equivalent physically mixed formulation. The incorporation of 1.5 % CF reinforcements dramatically improved both mechanical strength and thermal feedback. Notably, the composite with CF and a reduced NC content (2.5 %) achieved steady combustion with a regression rate ~ 45 % higher than the physical mixture benchmark. DIH confirmed that CFs intercept hot ejected agglomerates near the burning surface, increasing their average residence time from <0.5 ms (no CF) to ~5 ms with CF. Thermal analysis indicates that the conductive heat feedback to the unreacted layer, enhanced by the high thermal conductivity of CF and prolonged particle-surface contact, exceeded the required energy for continuous combustion in the CF-reinforced composites. These findings demonstrate that augmenting heat feedback through targeted structural and compositional design can effectively overcome combustion instabilities and substantially boost the energy release rate in high-loading nanoenergetic systems.

1. Introduction

Aluminum (Al) particles are widely used as energetic additives in propellants and pyrotechnics due to their high energy density [1,2]. However, Al nanoparticles (Al NPs) are prone to agglomeration and sintering during combustion, which dramatically reduces the accessible surface area and limits the reactivity gains expected from nanosizing [3–5]. One strategy to maintain the high surface area of nano metal fuels and improve the combustion of high-loading nano metals is to assemble the nanoparticles into mesoparticles using a low-temperature gas-generating binder (e.g., nitrocellulose, NC) that can disintegrate the agglomerates upon decomposition [6–12]. This basic premise is illustrated in Scheme 1 and has been directly imaged to validate this scheme [13].

Despite the advantages of mesoparticle assembly and their higher reactivity [6–11], when printed into a composite with polymer binders, the burning process is non-continuous. In particular, high-mesoparticle loadings, due to their superior reactivity, can actually lead to poor heat feedback to the reaction front from ejected fragments [6]. A recent study by Wang et al. investigated 3D-printed Al–CuO–NC mesoparticle composites (~90 wt% energetic content) and observed an unusual oscillatory combustion phenomenon characterized by periodic flame extinction and reignition at a stable frequency [6]. This oscillation was attributed to insufficient heat feedback to the unreacted layer during flame propagation: the intense gas release from the NC binder caused burning particle fragments to be ejected rapidly from the surface, depriving the reaction front of sustained heat due to their short residence time near the front [6]. The resulting loss of conductive feedback

* Corresponding author.
E-mail address: mrz@engr.ucr.edu (M.R. Zachariah).

https://doi.org/10.1016/j.cej.2025.171223
Received 8 August 2025; Received in revised form 3 November 2025; Accepted 23 November 2025
Available online 30 November 2025

left the underlying layer likely below its ignition threshold, leading to periodic flame extinction and reignition. The addition of carbon fibers (CFs) to the composite was found to eliminate the oscillations and enable continuous flame propagation by intercepting hot ejected particles and increasing thermal feedback [6,14–17]. However, even with CF reinforcement, the achieved regression rate in the mesoparticle composite was only comparable to that of an equivalent physically mixed Al–CuO formulation [6], indicating that the full potential of the mesoparticles' high reactivity had not yet been realized in their high-loading composites [6–11]. A synergistic approach that couples CF reinforcement with controlled adjustment of the polymer and gas-generator content to simultaneously enhance heat feedback and mitigate disruptive gas release is therefore expected to further improve the performance of mesoparticle composites.

In this work, we explore multiple approaches to manipulate the heat feedback and burning behavior of highly-loaded mesoparticle pyrolants. Mesoparticles composed of Al fuel, CuO oxidizer, and varying amounts of NC were prepared via spray-drying, then formulated into 3D-printed composite sticks using a polymer binder matrix (polymethyl methacrylate, PMMA, with hydroxypropyl methylcellulose, HPMC, in some cases to aid printability). We investigate the effects of (i) varying the polymer binder content (10–25 wt%), (ii) adding a small fraction (1.5 wt%) of CFs, and (iii) adjusting the NC content in the mesoparticles (to modulate gas release) on the combustion propagation. High-speed digital in-line holography (DIH) operated at 10^5 frames per second (fps), incorporated with three-color pyrometry, is employed to observe the flame propagation and quantify the statistical size, velocity, and residence time distributions of ejected burning fragments in each formulation. We also measure the mechanical properties (Young's modulus and tensile strength) of the printed composites to assess how structural integrity correlates with combustion behavior. By coupling CF reinforcement with NC regulation, we demonstrate that enhanced thermal feedback, achieved through improved mechanical cohesion and moderated gas generation, transforms the combustion of mesoparticle composites from an oscillatory regime to steady propagation, resulting in substantially higher regression rates than previously attainable. The findings of this study provide design guidelines for leveraging nanoscale energetics in practical formulations, emphasizing the critical role of heat feedback in achieving efficient, continuous combustion.

2. Methods

2.1. Mesoparticle preparation and 3D printing

Al–CuO–NC mesoparticles were synthesized via a spray-drying technique similar to that reported in prior works [7,9]. Aluminum nanoparticles (nominal diameter ~80 nm, 81 wt% active, NovaCentrix) and copper oxide nanoparticles (nominal diameter ~40 nm, US Research Nanomaterials) were mixed in a stoichiometric ratio and dispersed in NC solution (2.5–7.5 wt%) prepared using a solvent blend of *N*,*N*-dimethylformamide (DMF), isopropanol, and acetone (3:5:2 by volume). The NC was first obtained by drying collodion solution (Sigma–Aldrich), then dissolved in DMF before being mixed with the co-solvent blend. The resulting suspension was sonicated for 1 h to break agglomerates and stirred for at least 24 h to ensure uniform dispersion. The final mixture was spray-dried using a Büchi B290 mini spray dryer, with argon preheated to ~110 °C as the drying gas. To mitigate re-agglomeration during solvent evaporation, an in-line ultrasonication was used.

Printable inks were prepared by dissolving either 10–25 wt% PMMA (550,000 g·mol^{-1}, Alfa Aesar) or a mixture of 4 wt% PMMA and 6 wt% HPMC (Dow Chemical) in a 1:1 ethanol (Kopetec) / dichloromethane (Fisher Scientific) solvent, which dissolves the PMMA/HPMC but does not affect NC. Al–CuO–NC mesoparticles were added and ultrasonicated for 20 min, followed by 10-min mixing at 400 rpm in Thinky Mixer AR100. For composites with CF (diameter 7 μm, length ≈3 mm, Composite Envisions), 1.5 wt% CF was pre-dispersed into the PMMA/HPMC solution before mesoparticle addition. The inks were directly written through 14-gauge nozzles onto heated glass substrates at a constant speed of 2 mm·s^{-1}, and the printed 15-layer samples (~70 μm each layer) were cut into ~2-cm × 2-mm × 1-mm free-standing sticks. PMMA/HPMC was required for CF composites to prevent rapid sedimentation caused by the low viscosity of PMMA-only inks.

2.2. High-speed optical diagnostics with DIH and three-color pyrometry

The ejection of burning particles from the reaction zone was visualized using high-speed DIH. A collimated continuous-wave 532 nm laser (Coherent Verdi-V6) was used for illumination. The beam was spatially filtered through a 5-μm pinhole and expanded to a 25 mm diameter using a pair of plano-convex lenses with focal lengths of 10 mm and 100 mm (Thorlabs, models P5W, C060TMD-A, and LA1509-A, respectively). The resulting in-line holograms were recorded using a high-speed CMOS camera (Phantom VEO 1310S, binning mode) operating at 100,000 frames per second with an exposure time of 9 μs. Infinity K2 Distamax long-distance microscope lenses (NTX tube with CF-4 objective) were used to achieve a spatial resolution of 2.8 μm/pixel across a 0.90 × 0.67 mm field of view. To suppress broadband light emissions from the combustion zone, a narrow-band-pass optical filter (Thorlabs FLH532–4, 532 ± 2 nm) was installed in front of the detector. The optical focal plane was aligned between the fuel sample and the camera sensor to optimize the capture of diffraction patterns. The underlying principle of DIH is described in prior literature [18–20]. This configuration enabled high-contrast diffraction patterns generated by particles larger than ~3 μm to be captured and subsequently processed for three-dimensional tracking and sizing. The numerical reconstruction of particle fields was conducted using the Fresnel approximation [21], as expressed in Eq. (1):

$$I(x,y,z) = \left|\mathcal{F}^{-1}\left\{\mathcal{F}\left\{I_{ref}^{*}I_0(x,y)\right\}\cdot e^{i\frac{2\pi z}{\lambda}\sqrt{1-(\lambda f_x)^2-(\lambda f_y)^2}}\right\}\right| \quad (1)$$

where $I(x,y,z)$ is the reconstructed wave amplitude, $I_0(x,y)$ is the recorded hologram intensity, z is the distance from the particle reconstructed plane to the focal plane, λ is the laser wavelength (532 nm), f_x

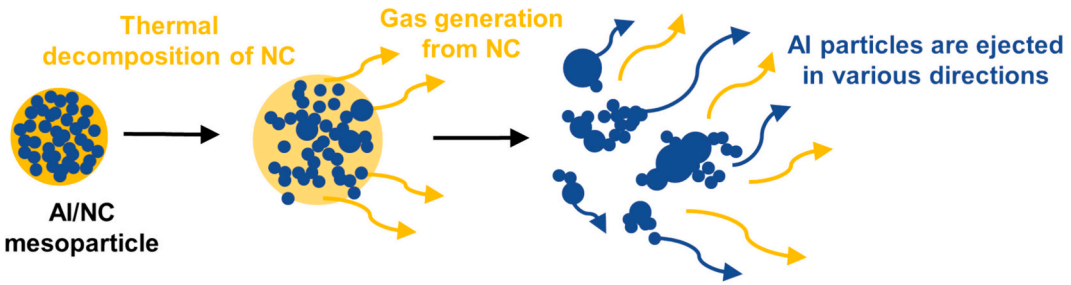

Scheme 1. Mechanism of enhanced combustion of mesoparticles (adapted with permission from Elsevier [13]).

and f_y are the transverse spatial frequencies in the x and y directions, respectively. The operators, $\mathscr{F}$ and $\mathscr{F}^{-1}$ denote the Fourier transform and inverse Fourier transform. Through this technique, we measured distributions of particle diameters, trajectories, and velocities in the vicinity of the burning surface for each formulation.

Combustion dynamics were recorded at both macroscopic and microscopic scales using high-speed color imaging, following methods described previously [22,23]. For macroscopic observations, a Phantom Miro 110 camera paired with a Nikon AF Micro Nikkor lens (aperture f/16) was used, yielding a spatial resolution of approximately 25 μm/pixel. Microscopic imaging was conducted with a Phantom VEO 710 L camera coupled to a long working distance microscope lens (Infinity Photo-Optical K2 DistaMax with CF-4 objective), achieving a spatial resolution of ~2.1 μm/pixel from a working distance of ~54 mm. Additionally, surface temperature evolution during combustion was monitored using a mid-wave infrared camera (Telops FAST M3K, resolution 30 μm·pixel^{-1}), as described in prior studies [6,24,25]. Three-color pyrometry was applied to the color imaging data to estimate surface temperatures across the field of view, following established techniques [26,27]. Raw red (R), green (G), and blue (B) intensity values were extracted by debayering the Bayer-patterned sensor output. Pixel-wise temperature estimation was performed by calculating intensity ratios between the color channels (G/R, B/G, and B/R) and comparing them to theoretical blackbody curves under the assumption of graybody emission. Calibration was conducted using blackbody sources (ThorLabs SLS201L and Micron M390), resulting in a temperature estimation uncertainty of ~200–300 K.

2.3. Tensile tests and SEM

The mechanical properties of the printed composites were evaluated through tensile testing [28,29]. A dual-column Instron 5969 testing machine was used to pull the printed sample strips (~30 mm × 2 mm × 0.5 mm) in tension until fracture at ~10 mm gauge length and 5 mm·min^{-1} crosshead speed. Young's modulus was determined from the initial linear slope of the stress–strain curve, and the ultimate tensile strength was recorded at break. The samples were also examined with a scanning electron microscope (FEI Nova NanoSEM 450).

3. Results and discussion

3.1. Effect of polymer binder content

Fig. 1(a) shows SEM micrographs of the 3D-printed mesoparticle composites of varying PMMA binder content (10, 15, and 20 % by weight). Higher binder loadings visibly increase the polymer adhesion between particles (for example, the 20 % PMMA sample exhibits thicker polymer bridges binding the mesoparticles, highlighted by yellow arrows in Fig. 1(a-3)). This increased cohesion with more binder was expected to improve structural integrity and potentially reduce the disruptive ejection of particles during combustion. The practical use of mesoparticles relies on preserving their structural integrity during the printing process. As shown in Fig. S1, the morphology and average size (3–5 μm) of the mesoparticles synthesized via spray-drying remain unchanged after incorporation into the printed composite. This observation confirms that the mesoparticles retain their integrity throughout the printing process.

Burning tests recorded by the high-speed camera revealed a strong influence of binder content on flame propagation. At 10 % and 15 % PMMA, the composites exhibited oscillatory combustion: the flame would repeatedly ignite and then extinguish, resulting in a "flashing" propagation as seen in the flame position vs. time traces (Fig. 1(b)) and transient regression rates (Fig. 1(c)). High-speed video snapshots for the 10 % PMMA case (Fig. 1(d)) show distinct phases of rapid burning followed by dark, extinguished intervals, after which the flame re-ignites further along the stick. The transient regression rates (instantaneous burn speeds calculated from dx/dt, where dt = 5 ms) during the active burning phases reached as high as ~1.6 cm·s^{-1} for 10 % PMMA and ~1.2 cm·s^{-1} for 15 % PMMA. However, due to the intermittent extinction, these fast bursts were interspersed with zero-regression intervals, bringing the average global propagation rates down to only ~0.11 cm·s^{-1} and ~ 0.22 cm·s^{-1} for 10 % and 15 % binder, respectively. Interestingly, the oscillation frequency increased with binder content, from roughly 7 Hz at 10 % PMMA to ~37 Hz at 15 % PMMA, suggesting that the presence of additional binder can lead to better combustion while imparting more cohesion. When the binder content was further raised to 20 %, the flame front advanced in a near-linear fashion (Fig. 1(b)), indicating a near-continuous combustion with no full extinguishment periods. Accordingly, the 20 % PMMA sample attained a higher global burn rate of ~0.28 cm·s^{-1}. This value is a significant improvement over the lower-binder cases; nevertheless, it remained

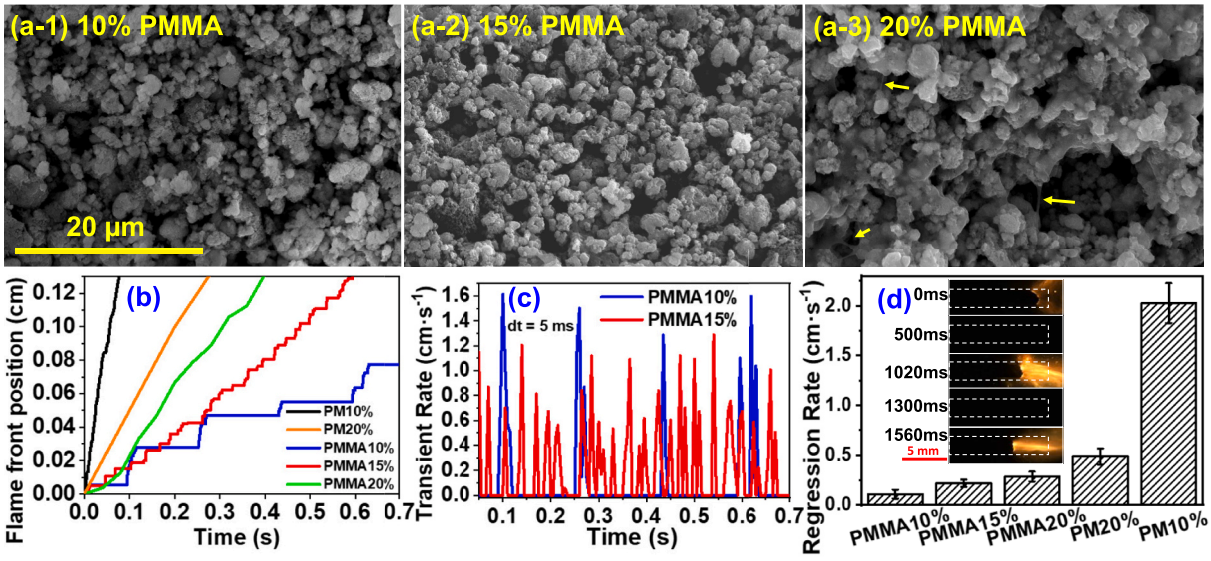

Fig. 1. (a) SEM of mesoparticle composites printed without CF; (b) flame front position and (c) transient regression rates at different times; (d) average global regression rates of the printed samples, including mesoparticle (PMMA 10–20 %) and physically-mixed Al-CuO composites (PM 10–20 %).

considerably lower than the burn rate of a benchmark physical mixture (Al + CuO + 7.5 % NC with 10 % PMMA binder, labeled PM10%) under the same test conditions (Fig. 1(d)). To distinguish whether this lower burn rate (compared to the PM10%) resulted from binder dilution or residual heat feedback limitations, we conducted an additional control test using a physically mixed composite with 20 % PMMA (PM20%). This control exhibited a burn rate of ~0.49 cm·s^{-1}, substantially slower than the physically mixed 10 %-PMMA sample (~2.0 cm·s^{-1}), confirming that binder dilution is the primary cause of the slow burn rate at higher polymer loadings. The fact that a simple physical mixture outperformed the mesoparticle composite at 20 % binder suggests that the advantages of the mesoparticle design were still not fully realized. Overall, the binder variation experiments show that increasing the polymer content can suppress severe oscillations and yield more stable combustion, but additional enhancements are needed to further accelerate the reaction.

High-speed DIH was employed to better understand the particle ejection dynamics underlying the oscillatory combustion. Fig. 2(a) illustrates the DIH setup used to capture particles ejected from the burning surface. An example hologram and reconstructed image of an ejected particle are given in Fig. 2(b). For the 10 % PMMA formulation, the holography results revealed that the average size of the ejected particles is about 15 μm (Fig. 2(c)). Considering fragments close to and smaller than the detection limit (2.8 μm/pixel) are not counted, the plotted distribution should be taken as an upper bound. These large burning fragments (mesoparticle agglomerates or flakes) were ejected from the surface at velocities on the order of a few m·s^{-1}. The distribution of particle velocities (Fig. 2(d)) showed an average ejection speed of approximately 3.0 m·s^{-1} for the 10 % binder composite, with most particles traveling in the direction opposite to flame propagation (the x-direction, ~2.7 m·s^{-1} on average) and smaller velocity components in perpendicular directions (~0.8 m·s^{-1} in y and z). Fig. 2(e) highlights a large burning flake (~300 μm in size) that left the combustion front. This particular flake was ejected relatively slowly (~0.11 m·s^{-1} initial velocity, due to its larger size) and was observed to explosively break apart into smaller pieces while in flight. At approximately 4.65 ms after ejection, the leading edge of the flake began reacting energetically, rapidly releasing numerous smaller particles. This intense reaction reduced the flake's forward velocity (in the x-direction) and caused it to momentarily reverse its trajectory. Almost simultaneously, a vigorous reaction commenced at the upper edge of the flake, accelerating it sharply downward (negative y-direction) and increasing its velocity to approximately 2.8 m·s^{-1} within the next 0.1 ms. Subsequently, the flake underwent rapid fragmentation, completely disintegrating and

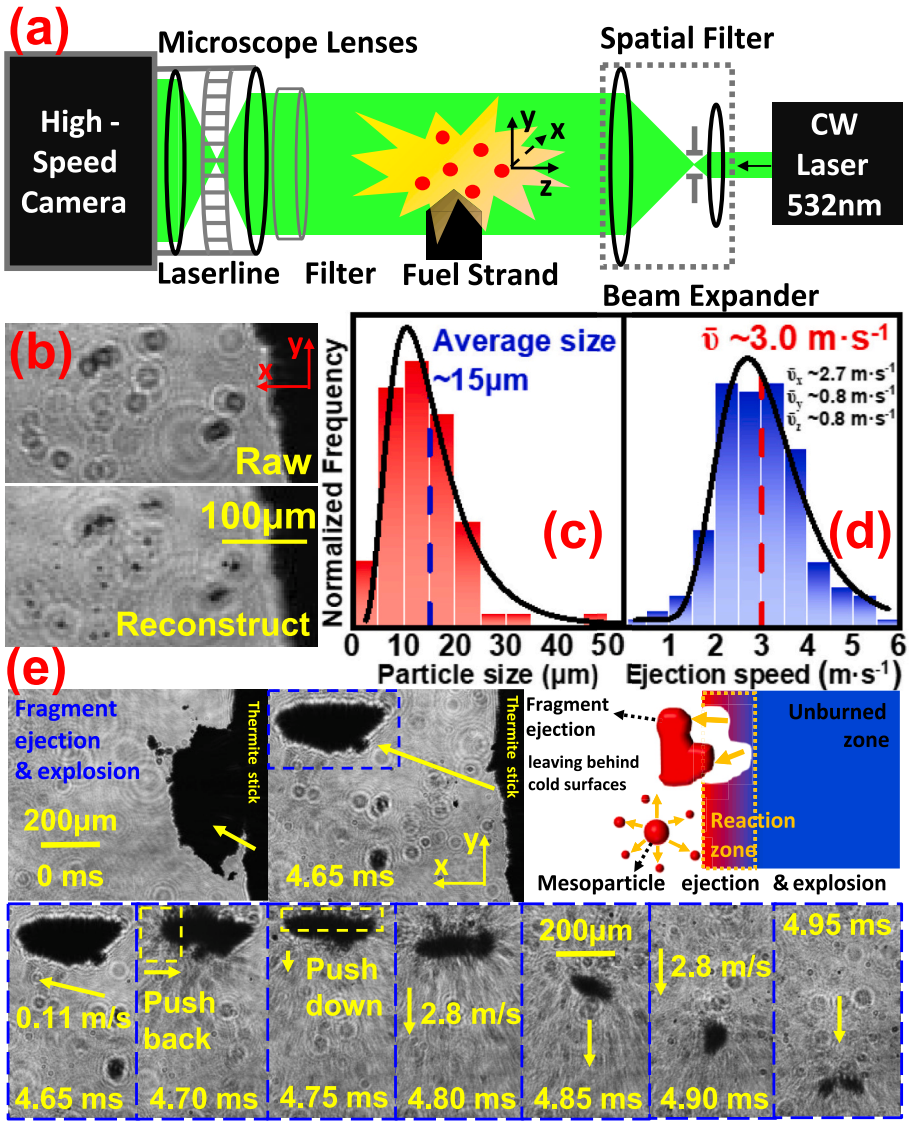

Fig. 2. (a) DIH setup illustration; (b) snapshot of raw and reconstructed holograms of ejected particles in 10 %-PMMA combustion; (c-d) corresponding size and velocity distribution of ejected particles; (e) DIH of a flying mesoparticle flake after it leaves the 10 %-PMMA pyrolant.

becoming undetectable within approximately 0.3 ms. Similar violent dynamics were frequently observed for particle ejections from the 10 % PMMA sample, highlighting that ejected particles remain highly reactive after leaving the pyrolant surface. This rapid reactivity results in minimal particle residence time and limited opportunity for effective heat transfer back to the unburned material, which explains the intermittent combustion behavior and lack of continuous flame propagation in these low-binder composites. More high-speed imaging results of these samples can be found in Figs. S2-S5.

In general, the DIH data confirmed that the oscillatory burning in low-binder composites is associated with the expulsion of burning materials from the reaction zone. Each time the flame was extinguished, a portion of the reacting material had effectively been blown off the surface, removing heat that would otherwise heat the next layer of fuel. Thus, mitigating the loss of burning fragments and improving heat feedback should lead to more continuous burning, so we proceed to test by introducing CFs in the composite.

3.2. Effect of CF on structural integrity and heat feedback

CFs were incorporated into the mesoparticle composites as a dual-purpose additive to improve mechanical strength and increase heat feedback [14]. A previous study (Shen et al. [30]) incorporating 5–10 μm carbon nanofibers into propellant composites reported no pronounced enhancement in tensile strength. Compared with commercial carbon nanotubes, whose lengths typically range from tens of nanometers to a few micrometers, CFs (3 mm in this work) provide millimeter-scale continuity, ensuring mechanical bridging and uninterrupted conduction across the burning front. Moreover, as discussed by Wang et al. [14], CFs initially distributed randomly tend to align parallel to the printing direction during extrusion through the needle, which is parallel to the flame propagation axis in the printed sticks. This alignment likely contributes to more efficient enhancement in mechanical strength and thermal feedback. The effect of CF length was investigated by Wang et al. [15] using both 3-mm and 25-μm CFs in nano-Al/NH_4ClO_4/HTPB composites, showing that the longer CFs provided better performance. Based on these comparisons, the present work used 3-mm CFs as the additive. Fig. 3(a) shows the influence of a 1.5 wt% CF addition on the mechanical properties of the printed 10 % PMMA/HPMC composite. Considering the dilution effect associated with higher polymer contents discussed in Section 3.1, all subsequent experiments were conducted using composites with 10 wt% polymer binder. With CF reinforcement, the tensile strength more than doubled (from ~0.65 MPa to ~1.3 MPa), and Young's modulus increased from ~180 MPa to ~600 MPa. These values were obtained from the representative stress–strain curves shown in Fig. 3(a). The SEM image inset in Fig. 3(a) (fracture cross-section) reveals CFs bridging across broken interfaces, confirming that the fibers were well integrated into the polymer/particle matrix and bore load during fracture. Given that structural integrity is essential for maintaining a coherent burning front under dynamic conditions, such reinforcement likely helps the composite withstand rapid internal pressurization caused by gas release during combustion, thereby preventing premature disintegration of the fuel matrix.

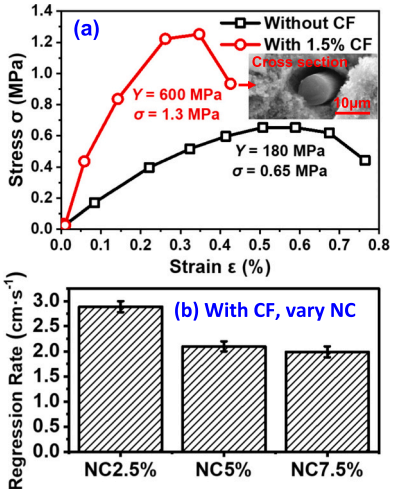

Fig. 3. (a) Tensile strength test on the samples with and without CF (mesoparticle +10 % PMMA/HPMC), where ε represents the strain percentage (ΔL/L), Y is the Young's modulus and σ is the tensile stress; (b) Regression rate after adding 1.5 % CF for mesoparticle pyrolants of different NC loadings (2.5–7.5 %). All composites are with 10 % polymer binders.

The introduction of CFs, coupled with adjustments in the mesoparticle NC content, led to markedly improved combustion performance. Fig. 3(b) summarizes the global regression rates of 3D-printed mesoparticle composites (with 10 % total PMMA/HPMC binder) containing 1.5 % CF, for several different NC loadings in the mesoparticles (ranging from 2.5 % to 7.5 % NC by weight in the solid mesoparticles). Overall, reducing the NC percentage (i.e., decreasing the gas generation) resulted in faster regression rates. With 7.5 % NC in the mesoparticles, the CF-containing composite still showed a moderate burn rate of ~2.0 $cm{\cdot}s^{-1}$. As the NC content was lowered, the propagation became progressively steadier. At the lowest NC level tested (2.5 % NC), the composite with CF achieved steady combustion with a regression rate of ~2.9 $cm{\cdot}s^{-1}$, about 45 % higher than that of the physical mixture reference. While excessive gas evolution can disrupt the flame front by ejecting burning fragments, a moderate level of gas release is still beneficial as it helps break apart agglomerates. Thus, NC plays a dual role, providing local dispersion but becoming detrimental when its gas output interrupts heat feedback. Based on our results, an intermediate NC fraction (~2.5 %) likely offers the best balance between these competing effects. This demonstrates that by simultaneously reinforcing the structure (via CF) and reducing the disruptive gas output (via lower NC in the mesoparticles), the mesoparticle composite can not only sustain continuous combustion but can also surpass the burn rate of the equivalent traditional formulation. These results underscore the role of less violent gas evolution in preserving the composite structure and retaining hot particles near the flame front, while CFs enhance both the mechanical stability and the thermal feedback necessary for sustaining high-rate combustion.

Direct evidence of the CFs' role in catching ejected particles was obtained through high-speed DIH. Fig. 4(a) presents a time sequence in which a CF (initial diameter ~ 7 μm) near the burning surface becomes gradually coated with leaving particles during combustion. At time 0 ms, the fiber became visible as the flame front neared. Over the next ~18 ms, numerous particles collide with and stick to the fiber (which is anchored in the composite), causing the effective fiber thickness to grow to ~50 μm. This dramatic thickening of the fiber indicates the accumulation of molten or partially reacted Al composite along its length, while the binding of Al onto CF might be due to the formation of Al-C bonds [16]. Recent molecular dynamics study by Zhou et al. [16] showed that at combustion temperatures (2500 K), 4-nm Al nanoparticles chemisorb strongly onto CF surfaces with an interaction energy of ~870 eV per particle, which is orders of magnitudes stronger than van-der-Waals adsorption at lower temperatures (~30 eV per particle at 1000 K), mainly due to formation of Al-C bonds within 40 ps of simulation time. This strong interfacial bonding substantially increases adhesion and suppresses particle rebound, prolonging the residence time of ejected Al fragments.

Fig. 4(b) zooms in on a single particle-capture event: a flake of Al composite (~200 μm across) is ejected from the flame front at 0.03 ms, travels a short distance, and then impacts the protruding end of a CF by 0.06 ms. Between 0.06 and 0.12 ms, the particle adheres to the fiber and oscillates/vibrates as it releases energy. By 0.45 ms, the particle residue has reshaped into a roughly spherical droplet attached to the fiber tip. This sequence confirms that CFs within the composite can effectively

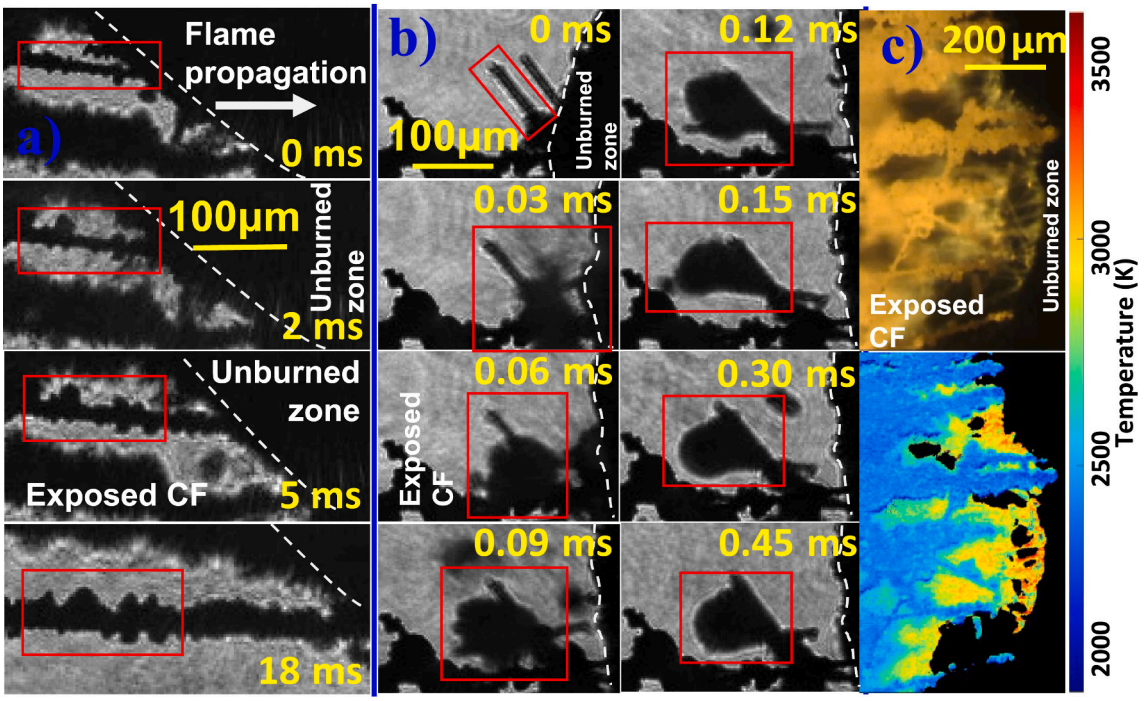

Fig. 4. Effect of the addition of 1.5 % CF (in mesoparticle +10 % PMMA/HPMC composite): (a) the growth of the thickness of CF as the pyrolant combusts; (b) the capture of a burning particle by the CFs; (c) high-speed three-color pyrometry showing temperature of flame front and CFs (temperature uncertainty 200-300 K). The dashed white lines indicate the location of the flame front. The dark areas on the right of these lines are unburned zones, while on the left are exposed CFs and ejected particles captured by CFs.

intercept flying burning fragments and hold them in place. The captured particles can burn to completion on the fiber, which means their heat is not lost to the far field but instead can conduct back into the nearby fuel. As a result, the residence time of hot agglomerates near the reaction front is greatly increased by the presence of CFs. Fig. 4(c) presents snapshots of the flame structure and corresponding pyrometry after addition of CFs. The average temperature of the flame front is ~2800 K (same as T_{flame} without CF in Fig. S4(b)), and the average temperature of CFs is ~2400 K. This slightly lower CF temperature reflects their role as thermally conductive bridges: They remain chemically stable over the short combustion timescale and do not participate in the thermite reaction. Instead, they continuously transfer heat from their exposed ends (heated by the attached burning fragments) into the cooler, unreacted layer. This process establishes a temperature gradient along the fiber, lowering its surface temperature relative to the reacting zone (by ~400 K) while sustaining conductive energy flow toward the substrate. The observed temperature difference confirms that CFs act as efficient thermal conduits, channeling the reaction heat backward to maintain

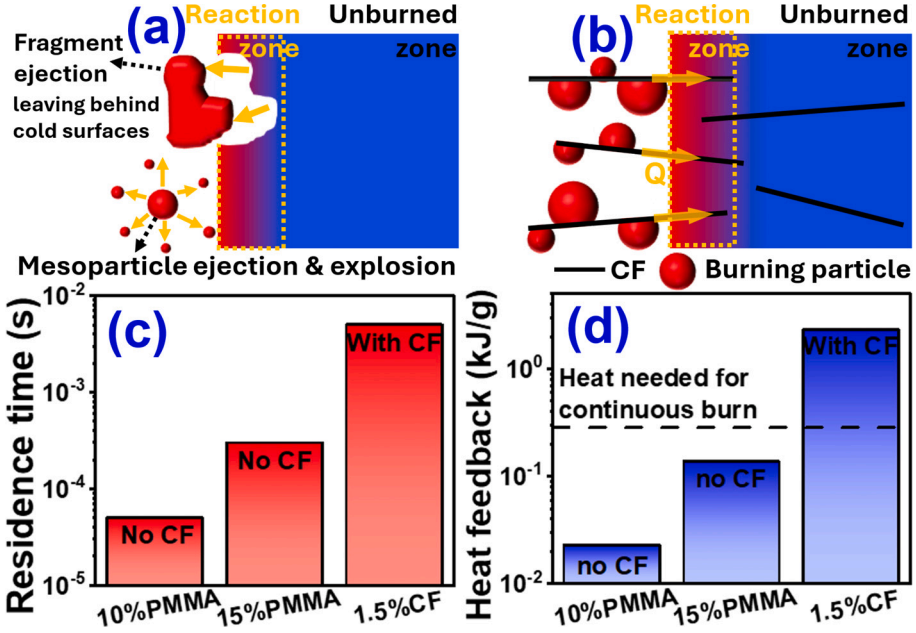

Fig. 5. Illustration on the burning mesoparticle pyrolant (a) without CF and (b) with CF; (c) Measured residence time and (d) estimated conduction heat feedback (upper limit) of mesoparticle pyrolants made with 10–15 % PMMA (no CF), or 10 % PMMA with CF.

preheating and promote continuous flame propagation.

From our high-speed imaging measurements, the average residence time (τ) of ejected particles on or near the surface was on the order of only ~0.05–0.3 ms for formulations without fibers (depending on binder content), whereas with CFs, this average residence time extended to the order of ~5 ms (before CFs break off). This order-of-magnitude increase in residence time provides significantly more opportunity for heat transfer from the hot particles to the unreacted substrate.

3.3. Calculation on the heat feedback enhancement

To quantify the effect of CFs on thermal feedback, we estimated the conductive heat transfer from burning particles to the unburned region for different cases [31–33], as illustrated in Fig. 5. The maximum conductive energy feedback ($Q_{feedback}$) from a hot particle to the adjacent substrate was estimated by Eq. (2):

$$Q_{feedback} = \frac{k \cdot \Delta T_1 \cdot \tau}{L} \tag{2}$$

where k is the effective thermal conductivity of the medium between the burning particle and the unreacted material, approximated using a series composite model that considers contributions from all components (PMMA binder, Al–CuO mesoparticles, and CFs). Because the polymer binder has the lowest thermal conductivity ($k_{PMMA} \sim 0.17$ W·m^{-1}·K^{-1} [34]), it dominates the overall thermal resistance in the series configuration. ΔT_1 is the temperature difference between the particle/flame (~2800 K, estimated by color imaging-pyrometry in Figs. 4 and S4) and the underlying unreacted material (~700 K, from IR measurements of the preheat zone [6]). L is the characteristic length of the conduction path, taken to be roughly the average particle diameter (~15 μm), which represents the typical distance over which heat must conduct from the hot-particle-flame interface to the underlying unreacted layer based on the particle-scale contact geometry observed in DIH (Figs. 2, 4). Using the CF diameter (~7 μm) as L would underestimate the conduction path, since the heat must traverse the particle–polymer interface before reaching the next reactive region. τ is the contact time (residence time) of the hot particle on the surface. Values of $L \approx 15$ μm and $T_{flame} \approx 2800$ K would yield an upper-bound estimate for heat feedback since we assume continuous contact and no heat losses.

We compared $Q_{feedback}$ to two other energy quantities: Q_{ig}, the energy required to raise a unit mass of the unreacted material from ambient/preheat temperature to its ignition temperature (~1050 K for this thermite composite) [33].

$$Q_{ig} = C_p \cdot \Delta T_2 \tag{3}$$

where C_p is the mass-weighted average of the composite specific heat, and $\Delta T_2 \sim 350$ K rise from 700 K to 1050 K. Q_{chem}, the energy released from complete reaction of that unit mass, is obtained from the reaction enthalpy of the Al + CuO thermite (~4.12 kJ·g^{-1}). For sustained, continuous combustion, one expects the condition $Q_{chem} > Q_{feedback} > Q_{ig}$ to be met [33]. In other words, the heat feedback to the unreacted portion must at least supply the ignition energy, and the chemical energy released must be sufficient to both provide that feedback and drive flame propagation. In all our formulations, the thermite's exothermicity (Q_{chem}) far exceeds what is required to heat the next layer by 350 K (Q_{ig}), by roughly a factor of 5. However, without CFs, the estimated $Q_{feedback}$ was found to be smaller than Q_{ig} in the oscillatory cases (for comparison, $Q_{feedback} \sim 0.023$ kJ·g^{-1} for 10 % PMMA, and ~ 0.14 kJ·g^{-1} for 15 % PMMA, while $Q_{ig} \sim 0.3$ kJ·g^{-1}), explaining the extinction between bursts. The burning particles did not remain in contact long enough to transfer sufficient energy before flying away.

The takeaway from this is that the combination of the higher thermal conductivity of CF (CFs have $k \sim 10$ W·m^{-1}·K^{-1} [14,15,35] vs. $k \sim 0.17$ W·m^{-1}·K^{-1} for the polymer binder [34]) and the increased residence time results in heat feedback, $Q_{feedback} \sim 8\times Q_{ig}$ for the 1.5 % CF case.

Fig. 5 summarizes this analysis by illustrating the different combustion scenarios: without CFs (Fig. 5(a)), burning fragments quickly depart and little heat is conducted back, whereas with CFs (Fig. 5(b)), particles are retained, and significant heat feedback occurs. The measured average residence times (Fig. 5(c)) and the corresponding estimated conductive feedback energies (Fig. 5(d)) clearly show the improvement due to CF addition. In short, adding CFs transforms the heat feedback condition from inadequate to sufficient, enabling the mesoparticle composite to reach a self-sustaining combustion regime.

4. Conclusion

In summary, we have demonstrated that the high reactivity leading to combustion instability of highly loaded Al–CuO–NC mesoparticle composites can be overcome through strategic modifications that enhance heat feedback to the reaction front. Increasing the polymer binder content from 10 % to 20 % was found to suppress the previously observed oscillatory (stop-and-go) combustion behavior, yielding a nearly continuous flame propagation. However, the burn rate in that case remained below that of an equivalent physically mixed thermite, highlighting the need for further improvement. By incorporating a small fraction of CFs (1.5 wt%) and simultaneously reducing the gas-generating NC content within the mesoparticles, we achieved a significantly enhanced combustion performance: the modified composite burned steadily with a regression rate approximately 45 % higher than the physical mixture benchmark. Our approaches of tuning gas-releasing binder in mesoparticle and CF reinforcements address particle aggregation, macroscopic structural integrity, and retention of reactive fragments. In contrast, state-of-the-art engineered approaches of nanoenergetics such as multilayer films and core–shell particles [5,36,37] often enhance combustion performance via improved mass-transport and rapid interfacial reaction by (i) reducing or bypassing the native oxide layer (like reactive coatings, eutectic-melting bilayers), or (ii) creating well-defined nanoscale contact areas that favor ultrafast energy release. These architectures typically require specialized fabrication (layer deposition or complex surface chemistry) and are complementary to the mesoparticle and CF-reinforced strategies explored in this work.

Mechanistically, CFs provide structural reinforcement and act as thermal conduits and traps for hot particles. The CF-reinforced composites exhibited a doubling of tensile strength and a tripling of modulus, indicating a much greater resistance to cracking or blow-off during combustion. High-speed holographic imaging confirmed that CFs intercept ejected reactive fragments and hold them in place, prolonging their exposure to the unreacted material. This effectively increases the conductive heat transfer into the next fuel layer, which we quantified through simplified heat feedback calculations. The analyses showed that without fibers, the brief contact of burning particles yielded insufficient heat feedback ($Q_{feed} < Q_{need}$), explaining the flame extinction in low-binder formulations. With fibers, the greatly extended particle residence time and higher thermal conductivity pathways raised Q_{feed} toward or above the threshold required to ignite the unburned composite, thereby sustaining continuous combustion. Overall, the integration of CF networks and the tuning of internal gas release provide a viable route to unlocking the full energy potential of mesoparticle-based energetics. These findings underscore the critical role of heat feedback in propagating reactions of nanoenergetic composites.

CRediT authorship contribution statement

Lei Yang: Writing – original draft, Visualization, Data curation. **Keren Shi:** Writing – review & editing, Data curation. **Yuxin Zhou:** Writing – review & editing, Data curation. **Mahbub Chowdhury:** Data curation. **Afrida Anis:** Writing – review & editing, Data curation. **Michael R. Zachariah:** Writing – review & editing, Resources, Project administration, Methodology, Investigation, Funding acquisition,

Conceptualization.

Declaration of competing interest

The authors declare no conflict of interest.

Data availability

Data will be made available on request.

Acknowledgments

This work was supported by the DTRA-MSEE URA and the AFOSR.

Appendix A. Supplementary data

Supplementary data to this article can be found online at https://doi.org/10.1016/j.cej.2025.171223.

References

[1] E.L. Dreizin, Metal-based reactive nanomaterials, Prog. Energy Combust. Sci. 35 (2009) 141–167, https://doi.org/10.1016/j.pecs.2008.09.001.
[2] K. Sullivan, G. Young, M.R. Zachariah, Enhanced reactivity of nano-B/Al/CuO MIC's, Combust. Flame 156 (2009) 302–309, https://doi.org/10.1016/j.combustflame.2008.09.011.
[3] D. Sundaram, V. Yang, R.A. Yetter, Metal-based nanoenergetic materials: synthesis, properties, and applications, Prog. Energy Combust. Sci. 61 (2017) 293–365, https://doi.org/10.1016/j.pecs.2017.02.002.
[4] K.T. Sullivan, N.W. Piekiel, C. Wu, S. Chowdhury, S.T. Kelly, T.C. Hufnagel, K. Fezzaa, M.R. Zachariah, Reactive sintering: an important component in the combustion of nanocomposite thermites, Combust. Flame 159 (2012) 2–15, https://doi.org/10.1016/j.combustflame.2011.07.015.
[5] L. Yang, Y. Zhou, M. Chowdhury, Y. Qin, M.M. Dickson, M.R. Zachariah, Synergistic transition multi-metal coatings drive sub-melting-point reaction of aluminum, Chem. Eng. J. 519 (2025) 164794, https://doi.org/10.1016/j.cej.2025.164794.
[6] Y. Wang, M. Chowdhury, Y. Zhou, G. Issac Paul, K. Shi, M.R. Zachariah, Oscillating-to-continuous combustion transition in mesoparticle composites through manipulation of heat feedback, Adv. Funct. Mater. (2024) 2406722, https://doi.org/10.1002/adfm.202406722.
[7] R.J. Jacob, B. Wei, M.R. Zachariah, Quantifying the enhanced combustion characteristics of electrospray assembled aluminum mesoparticles, Combust. Flame 167 (2016) 472–480, https://doi.org/10.1016/j.combustflame.2015.09.032.
[8] G. Young, H. Wang, M.R. Zachariah, Application of nano-aluminum/nitrocellulose mesoparticles in composite solid rocket propellants, Propellants, Explos., Pyrotech. 40 (2015) 413–418, https://doi.org/10.1002/prep.201500020.
[9] M. Chowdhury, P. Ghildiyal, A. Rojas, Y. Wang, H. Wang, M.R. Zachariah, High-yield spray drying assembly and reactive properties of nanoenergetic mesoparticle composites, Adv. Powder Technol. 34 (2023) 104075, https://doi.org/10.1016/j.apt.2023.104075.
[10] S. Chen, Z. Tang, K. Tang, L. Cui, Z. Qin, K. Xu, Lowering the burning rate temperature coefficient of composite propellant by compensating its burning surface through thermal expansion and contraction in microstructure, Chem. Eng. J. 494 (2024) 152800, https://doi.org/10.1016/j.cej.2024.152800.
[11] P.M. Guerieri, J.B. DeLisio, M.R. Zachariah, Nanoaluminum/nitrocellulose microparticle additive for burn enhancement of liquid fuels, Combust. Flame 176 (2017) 220–228, https://doi.org/10.1016/j.combustflame.2016.10.011.
[12] Z. Tang, S. Chen, H. Yu, K. Tang, Z. Qin, F. Zhao, K. Xu, Regulation of catalysts on tightly packaged solid propellant energetic particles: high combustion performance with low temperature sensitivity, Langmuir 40 (2024) 18122–18132, https://doi.org/10.1021/acs.langmuir.4c01716.
[13] Y. Zhou, K. Shi, M. Chowdhury, E. Hagen, Y. Wang, M.R. Zachariah, Direct microscopic imaging of exploding aluminum/nitrocellulose mesoparticles to reveal the enhanced combustion mechanism, Fuel 387 (2025) 134348, https://doi.org/10.1016/j.fuel.2025.134348.
[14] H. Wang, D.J. Kline, M.C. Rehwoldt, M.R. Zachariah, Carbon fibers enhance the propagation of high loading nanothermites: in situ observation of microscopic combustion, ACS Appl. Mater. Interfaces 13 (2021) 30504–30511, https://doi.org/10.1021/acsami.1c02911.
[15] H. Wang, E. Hagen, K. Shi, S. Herrera, F. Xu, M.R. Zachariah, Carbon fibers as additives to engineer agglomeration and propagation of aluminized propellants, Chem. Eng. J. 460 (2023) 141653, https://doi.org/10.1016/j.cej.2023.141653.
[16] Y. Zhou, M.R. Zachariah, Molecular dynamics study on the capture of aluminum particles by carbon fibers during the propagation of aluminum-based energetics, Energy Fuel 38 (2024) 8992–9000, https://doi.org/10.1021/acs.energyfuels.4c00832.
[17] K. Shi, Y. Wang, G.I. Paul, M.R. Zachariah, The influence of heat feedback and thermal conductivity on the burn rate of thermite composites, Combust. Flame 269 (2024) 113593, https://doi.org/10.1016/j.combustflame.2024.113593.
[18] Y. Chen, D.R. Guildenbecher, K.N.G. Hoffmeister, M.A. Cooper, H.L. Stauffacher, M.S. Oliver, E.B. Washburn, Study of aluminum particle combustion in solid propellant plumes using digital in-line holography and imaging pyrometry, Combust. Flame 182 (2017) 225–237, https://doi.org/10.1016/j.combustflame.2017.04.016.
[19] J. Huang, S. Li, W. Cai, Y. Qian, E. Berrocal, M. Aldén, Z. Li, Quantification of the size, 3D location and velocity of burning iron particles in premixed methane flames using high-speed digital in-line holography, Combust. Flame 230 (2021) 111430, https://doi.org/10.1016/j.combustflame.2021.111430.
[20] Y.C. Mazumdar, M.E. Smyser, J.D. Heyborne, M.N. Slipchenko, D. R. Guildenbecher, Megahertz-rate shock-wave distortion cancellation via phase conjugate digital in-line holography, Nat. Commun. 11 (2020) 1129, https://doi.org/10.1038/s41467-020-14868-y.
[21] U. Schnars, C. Falldorf, J. Watson, W. Jüptner, Digital holography, in: U. Schnars, C. Falldorf, J. Watson, W. Jüptner (Eds.), Digital Holography and Wavefront Sensing: Principles, Techniques and Applications, Springer Berlin Heidelberg, Berlin, Heidelberg, 2015, pp. 39–68, https://doi.org/10.1007/978-3-662-44693-5_3.
[22] Y. Wang, E. Hagen, P. Biswas, H. Wang, M.R. Zachariah, Imaging the combustion characteristics of Al, B, and Ti composites, Combust. Flame 252 (2023) 112747, https://doi.org/10.1016/j.combustflame.2023.112747.
[23] H. Wang, B. Julien, D.J. Kline, Z. Alibay, M.C. Rehwoldt, C. Rossi, M.R. Zachariah, Probing the reaction zone of nanolaminates at ~μs time and ~μm spatial resolution, J. Phys. Chem. C 124 (2020) 13679–13687, https://doi.org/10.1021/acs.jpcc.0c01647.
[24] K. Shi, M. Bokhoor, Y. Wang, T.P. Weihs, M.R. Zachariah, Propagation rate and product modulation in SHS reactions via focused microwave heating, Chem. Eng. Sci. 302 (2025) 120794, https://doi.org/10.1016/j.ces.2024.120794.
[25] K. Shi, Y. Wang, M.R. Zachariah, Microwave antenna focusing for spatially resolved modulation of burn rate, Chem. Eng. J. 492 (2024) 152192, https://doi.org/10.1016/j.cej.2024.152192.
[26] D.J. Kline, M.C. Rehwoldt, J.B. DeLisio, S.C. Barron, H. Wang, Z. Alibay, J. C. Rodriguez, G.M. Fritz, M.R. Zachariah, In-operando thermophysical properties and kinetics measurements of Al-Zr-C composites, Combust. Flame 228 (2021) 250–258, https://doi.org/10.1016/j.combustflame.2020.12.045.
[27] R.J. Jacob, D.J. Kline, M.R. Zachariah, High speed 2-dimensional temperature measurements of nanothermite composites: probing thermal vs. gas generation effects, J. Appl. Phys. 123 (2018), https://doi.org/10.1063/1.5021890.
[28] H. Wang, J. Shen, D.J. Kline, N. Eckman, N.R. Agrawal, T. Wu, P. Wang, M. R. Zachariah, Direct writing of a 90 wt% particle loading nanothermite, Adv. Mater. 31 (2019) 1806575, https://doi.org/10.1002/adma.201806575.
[29] H. Wang, M. Rehwoldt, D.J. Kline, T. Wu, P. Wang, M.R. Zachariah, Comparison study of the ignition and combustion characteristics of directly-written Al/PVDF, Al/Viton, and Al/THV composites, Combust. Flame 201 (2019) 181–186, https://doi.org/10.1016/j.combustflame.2018.12.031.
[30] J. Shen, Z. Liu, B. Xu, H. Liang, Y. Zhu, X. Liao, Z. Wang, Influence of carbon nanofibers on thermal and mechanical properties of NC-TEGDN-RDX triple-base gun propellants, Propellants, Explos., Pyrotech. 44 (2019) 355–361, https://doi.org/10.1002/prep.201800257.
[31] A. Ishihara, M.Q. Brewster, T.A. Sheridan, H. Krier, The influence of radiative heat feedback on burning rate in aluminized propellants, Combust. Flame 84 (1991) 141–153, https://doi.org/10.1016/0010-2180(91)90043-B.
[32] G.C. Egan, M.R. Zachariah, Commentary on the heat transfer mechanisms controlling propagation in nanothermites, Combust. Flame 162 (2015) 2959–2961, https://doi.org/10.1016/j.combustflame.2015.04.013.
[33] D.J. Kline, Z. Alibay, M.C. Rehwoldt, A. Idrogo-Lam, S.G. Hamilton, P. Biswas, F. Xu, M.R. Zachariah, Experimental observation of the heat transfer mechanisms that drive propagation in additively manufactured energetic materials, Combust. Flame 215 (2020) 417–424, https://doi.org/10.1016/j.combustflame.2020.01.020.
[34] Y. Agari, A. Ueda, Y. Omura, S. Nagai, Thermal diffusivity and conductivity of PMMA/PC blends, Polymer 38 (1997) 801–807, https://doi.org/10.1016/S0032-3861(96)00577-0.
[35] W. Nasri, Z. Driss, R. Djebali, K.-Y. Lee, H.-H. Park, A. Bezazi, P.N.B. Reis, Thermal study of carbon-fiber-reinforced polymer composites using multiscale modeling, Materials 16 (2023) 7233, https://doi.org/10.3390/ma16227233.
[36] Y. Zhou, L. Yang, A.K. Vasudevan, M. Dickson, M. Chowdhury, K. Shi, M. R. Zachariah, Nickel-coated aluminum nanoparticles for modulating ignition temperature: interfacial chemistry and mechanism, ACS Appl. Eng. Mater. 3 (2025) 2346–2353, https://doi.org/10.1021/acsaenm.5c00272.
[37] C. Zhang, Y. Kou, L. Xiao, Y. Hu, Q. Lu, F. Zhao, Y. Hu, W. Jiang, Y. Yang, G. Hao, Research progress on the modification of B and Al high-energy fuels for powder fuel ramjet applications, ACS Appl. Mater. Interfaces 17 (2025) 11522–11551, https://doi.org/10.1021/acsami.4c18379.